RESEARCH

# Brittleness index evaluation of gas-bearing sandstone under triaxial compression conditions

Jun Wang · Jiahui Du · Wenpu Li · Xianhui Chen · Huan Zhang · Tao Wang · Zhu Li · Ruiqing Hao

**Abstract** Brittleness is a critical property in gas-bearing rock excavation and reservoir fracturing. This paper analyzes the three types of brittleness indices in detail, proposes new indices, and conducts relevant conventional triaxial tests for analysis. A stress–strain curve-based brittleness index would be appropriate for the evaluation of brittleness if the parameters represented unique and certain stress–strain curves. Therefore, a new brittleness index is proposed. It consists of two components: the stress variation index and the strain variation index, which reflects the strain ratio of the stress drop and the relationship between elastic and post-peak strains, combining the stress variation and strain variation in the pre- and post-peak phases. Triaxial compression tests of sandstone under different confining pressures and gas pressures were conducted, and specific stress and strain parameters were collected. Based on the comparison and analysis of various brittleness indices, it is found that the newly proposed brittleness index can be a good measure of the brittle evolution of sandstones under different confining pressures and gas pressures, and it can provide a more accurate estimate of rock brittleness than the existing indices. The index is also used to further investigate the relationship between rock brittleness and confining and gas pressures. This has important implications for the assessment of rock brittleness in practical engineering.

## Article Highlights

- Sandstone ratio stress and strain parameters were obtained by triaxial compression tests.
- A new index is proposed based on stress drop and strain ratio.
- The relationship between rock brittleness and the surrounding pressure and gas pressure was investigated.

J. Wang · J. Du · W. Li (✉) · X. Chen · H. Zhang ·
T. Wang
College of Safety and Emergency Management
Engineering, Taiyuan University of Technology,
Taiyuan 030024, China
e-mail: liwenputyut@163.com

W. Li
Key Laboratory of Shanxi Province for Mine Rock Strata
Control and Disaster Prevention, Taiyuan 030024, China

W. Li
Shanxi Province Coal-Based Resources Green
and High-Efficiency Development Engineering Center,
Taiyuan 030024, China

Z. Li · R. Hao
College of Mining Engineering, Taiyuan University
of Technology, Taiyuan 030024, China

Springer

# 1 Introduction

Characterization of brittleness is crucial to applications in rock excavation engineering and unconventional gas exploration activities, such as borehole collapse and hydraulic fracturing (Meng et al. 2015; Holt et al. 2015; Rybacki et al. 2016; Zhang et al. 2016). Generally, the failure of brittle rock is associated with a sudden drop in stress, even the possibility of rock debris splintering. For different engineering applications with reservoir rocks, this failure must be effectively controlled to either promote or restrain its effects. Therefore, a robust understanding of brittleness can provide important insights for more successful reservoir design.

A number of researchers have explored the measurement of brittleness through a variety of different methods (Meng et al. 2015; Rybacki et al. 2016; Zhang et al. 2016; Hucka and Das 1974; Yagiz 2009; Holt et al. 2011). Among these methods, broadly, there are three approaches to estimating and classifying brittleness. One approach is based on stress–strain curves, which incorporate variables for strength, deformation, and energy (Meng et al. 2015; Zhang et al. 2016; Tarasov and Potvin 2013). Another approach is based on physical and mechanical characteristics related to the Young's modulus, Poisson's ratio, mineral composition, porosity, friction angle and hardness of the material (Hucka and Das 1974; Yagiz 2009). The third approach is based on the response of special test parameters to excavation operations, such as the punch penetration test (Yagiz 2009) and the point load test (Khadivi et al. 2023). Furthermore, the distinction and transition between brittle and ductile behavior have been evaluated with ductility considered to be the opposite deformation behavior to brittleness (Rybacki et al. 2016; Tarasov and Potvin 2013); however, no consensus has yet been reached on the precise definition or method of measurement of rock brittleness.

Rock brittleness is also influenced by certain boundary conditions, such as the stress loading path, confining pressure, pore pressure, temperature and differential stress (Rybacki et al. 2015). In particular, pore pressure significantly impacts rock deformation, permeability, strength and brittleness. Wu et al. (2019) used a coupled FEM-DEM method to analyse the effects of confining pressure on the rock-crushing process, rock-crushing efficiency and post-crushing debris distribution. Chen et al. (2013) used numerical analysis software to numerically simulate the effect of confining pressure on the occurrence of transverse fractures in rock. Liu (2013) found that the strength of the fine sandstone increased with increasing confining pressure. Chen et al. (2012) observed that as confining pressure increased in the unloaded state, the energy dissipation for the same transverse deformation increased and the rock samples became more brittle. Change in stress or pore gas pressure is regarded as a key factor for mechanical and permeability behaviors (Pan and Connell 2007; Liu et al. 2011; Xie et al. 2015). The effects of the saturation pressures of water, nitrogen and carbon dioxide on the strength of coal samples have been investigated in uniaxial compression tests (Ranjith et al. 2010; Perera et al. 2011; Vishal et al. 2015). Xue et al. (2022) used mercury intrusion tests, wave velocity tests and triaxial compression tests to reveal changes in the microstructure and mechanical properties of low-permeability coals under fatigue fracturing tests. Xue et al. (2023) used triaxial compression tests and acoustic emission (AE) tests to evaluate the effect of $CO_2$ adsorption pressure on the mechanical properties of coal blocks. Zhang et al. (2020) found that the strength of the briquettes decreased with increasing gas pressure, while the absolute deformation of the briquettes increased. Wang et al. (2019) found that the stress–strain curve tends to increase and then decrease throughout the stress–strain of coal, while the permeability-strain curve tends to decrease and then increase. Xu et al. (2020) found the relationship between permeability, porosity and hydrostatic pressure to be exponential and power functions, respectively, by conducting triaxial tests. Du et al. (2018) found that at lower pressure-bearing conditions, the cumulative AE counts and energies of gas-bearing coal bodies were higher than those of gas-bearing coal bodies. Li et al. (2021) consider different fracture evolutions in favour of a link with gas pressure. Bai et al. (2020) investigated the pore structure evolution characteristics of coal under different CPTJ pressures. It has been determined that the strength of rock infiltrated by gas decreases because of the effect of gas adsorption, which also decreases the rock's brittleness (Yin et al. 2015a, b; Kong et al. 2015; Li et al. 2022a, b). Therefore, pore pressure should be considered in the determination of rock brittleness. Of course, other aspects can also have an effect on rock brittleness. Li

et al. (2022a, b) found a gradual decrease in brittleness and an increase in ductility at high temperatures in quartz-rich sandstones. Wang et al. (2022) discovered that the degree of reconsolidation significantly affects the tendency of excess pore water pressure ratio to vary with increasing number of cyclic loads. Duan et al. (2021) investigated the effect of brittleness under true triaxial conditions. However, these effects are not the focus of this paper's research.

In this paper, previously described indices for evaluating rock brittleness are first summarized, and the calculation method of each index is defined. Then, based on various existing methods of assessment, a new method for estimating rock brittleness is proposed based on the stress–strain curve. Experimental data is collected from standard triaxial compression tests under different confining pressures and pore gas pressures. Finally, the associated brittleness index values are calculated and analyzed.

## 2 Summary and evaluation of previous approaches for brittleness evaluation

Rock brittleness indices have received increasing attention in recent years. Many researchers have conducted studies into the concept and measurement methods of rock brittleness, which is a property based on a combination of various rock mechanical parameters (Dursun and Gokay 2016). Three categories of brittleness index methodologies have been explored. One approach is to define the index in terms of stress–strain behaviors, including strength, deformation and energy. Another approach is to describe the index in terms of physical and mechanical characteristics related to the Young's modulus, Poisson's ratio, mineral composition, porosity, friction angle and hardness of the material. The third approach is to evaluate the responses of special test parameters to excavation operations, which include the punch penetration test, impact test and point load test. The descriptions and formulae of previously defined brittleness indices are listed in Table 1.

### 2.1 Brittleness indices based on stress–strain behaviors

The stress–strain relationship is widely known and fundamental for determining the mechanical deformation and strength properties of porous rock. A stress–strain curve always refers to both pre- and post-peak behaviors. Accordingly, the deformation performance and strength characteristics of both the pre-peak and post-peak regimes should be considered for the evaluation of rock brittleness with this approach. The differences between brittleness indices thus reflect different deformation and strength values before and after rock failure.

Brittleness can be defined based on the strength properties of brittle rocks. The brittleness indices $B_1$, $B_2$ and $B_3$ are defined based on uniaxial compressive strength (UCS) and Brazilian tensile strength (BTS). These three indices express strength ratios, convenient for rock mechanics. The relationship between compressive strength and tensile strength has been examined and discussed by Hucka and Das (1974), Yagiz (2009), and Altindag (2002), who reported that tensile strength shows a near-linear increasing trend with increasing compressive strength. Additionally, the results of these studies indicate that the range of variation in the value of $B_1$ is small. Because of this limitation, $B_1$ is not sensitive enough to assess rock brittleness accurately. $B_2$ encounters the same problem because it can also be expressed in terms of $B_1$. Moreover, these three indices do not account for confining pressure. The correlations between uniaxial compressive strength, Brazilian tensile strength and rock density are used to determine the brittleness index $B_4$, and it was found that this expression produced accurate estimates (Yagiz 2009). Bishop (1967) suggested an approach for the assessment of rock brittleness that incorporates the relationship between peak shear strength and the residual shear strength under triaxial compression: the brittleness index $B_5$ is calculated using the ratio between the reduction in strength and peak shear strength. This index is influenced by confining pressure because these two strength values are both dependent upon confining pressure. Consequently, the mechanical behavior of rock indicated by this index would transition from brittle failure to ductile failure with increasing confining pressure (Rickman et al. 2008; Yang et al. 2013). In conventional triaxial experiments, when the values of $\tau_p$ and $\tau_r$ are similar, B5 is close to 0, which indicates that the rock is ductile; when the values of $\tau_p$ and $\tau_r$ differ greatly, B5 is close to 1, which indicates that the rock is brittle. However, this way of describing brittleness relies only on the rock stress path and

**Table 1** Summary of previously defined brittleness indices

| Formulae | Variable descriptions | Test methods | References |
|---|---|---|---|
| $B_1 = \frac{\sigma_c}{\sigma_t}$ | $\sigma_c$ is the unconfined compressive strength | UCS and BTS tests | Hucka and Das (1974) |
| $B_2 = \frac{\sigma_c - \sigma_t}{\sigma_c + \sigma_t}$ | $\sigma_t$ is the Brazilian tensile strength | As above | Altindag (2002) |
| $B_3 = \frac{\sigma_c \cdot \sigma_t}{2}$ | | As above | Yagiz (2009) |
| $B_4 = 0.198\sigma_c - 2.174\sigma_c + 0.913\rho - 3.807$ | $\rho$ is the rock density | As above | Yagiz (2009) |
| $B_5 = \frac{\tau_p - \tau_r}{\tau_p}$ | $\tau_p$ is the peak shear strength $\tau_r$ is the residual shear strength | Stress–strain tests | Bishop (1967) |
| $B_6 = \frac{\varepsilon_{el}}{\varepsilon_{tot}}$ | $\varepsilon_{el}$ is the elastic strain $\varepsilon_{tot}$ is the total strain at failure | As above | Hucka and Das (1974) |
| $B_7 = \frac{\varepsilon_r - \varepsilon_p}{\varepsilon_r}$ | $\varepsilon_r$ is the residual strain $\varepsilon_p$ is strain at failure | As above | Rybacki et al. (2016) |
| $B_8 = \frac{\varepsilon_f^p - \varepsilon_c^p}{\varepsilon_c^p}$ | $\varepsilon_f^p$ is the plastic strain when the friction strength is fully mobilized, $\varepsilon_c^p$ is the plastic strain when the cohesive strength reaches the residual strength value | As above | Hajiabdolmajid and Kaiser (2003) |
| $B_9 = \frac{W_{el}}{W_{tot}}$ | $W_{el}$ is the elastic energy $W_{tot}$ is the total energy at failure | As above | Hucka and Das (1974) |
| $B_{10} = \frac{M - E}{M}$ | $E$ is the unloading elastic modulus $M$ is the post-peak elastic modulus | As above | Tarasov and Potvin (2013) |
| $B_{11} = \frac{E}{M}$ | | As above | Tarasov and Potvin (2013) |
| $B_{12} = B_{1d}B_{2d} = \frac{\sigma_p - \sigma_r}{\sigma_p} \frac{1}{10}\log\left\|\frac{\sigma_p - \sigma_r}{\varepsilon_p - \varepsilon_r}\right\|$ | $\frac{\sigma_p - \sigma_r}{\sigma_p}$ represents the stress drop magnitude, $\frac{1}{10}\log\left\|\frac{\sigma_p - \sigma_r}{\varepsilon_p - \varepsilon_r}\right\|$ represents the stress drop velocity | As above | Meng et al. (2015) |
| $B_{13} = \frac{1}{2}\left(\frac{E - E_{min}}{E_{max} - E_{min}} + \frac{\nu_{max} - \nu}{\nu_{max} - \nu_{min}}\right)$ | $E_{max}$ and $E_{min}$ are the maximum and minimum values of the Young's modulus; $\nu_{max}$ and $\nu_{min}$ are the maximum and minimum values of the Poisson's ratios | Physical characteristics tests | Rickman et al. (2008) |
| $B_{14} = \frac{E}{\nu}$ | $E$ is the Young's modulus $\nu$ is the Poisson's ratio | As above | Luan et al. (2014) |
| $B_{15} = \frac{E\rho}{\nu}$ | | As above | Sun et al. (2013) |
| $B_{16} = \frac{W_Q}{W_Q + F_C + W_{Cl}}$ | $W_Q$ is the weight of quartz $W_C$ is the weight of carbonate | Mineralogical analysis | Jarvie et al. (2007) |
| $B_{17} = \frac{W_Q + W_{Dol}}{W_Q + W_{Dol} + W_{Lm} + W_{Cl} + W_{TOC}}$ | $W_{Cl}$ is the weight of clay minerals $W_{Dol}$ is the weight of dolomite | As above | Wang and Gale (2009) |
| $B_{18} = \frac{W_Q + W_{Cb}}{W_Q + W_{Cb} + W_{Cl} + W_{TOC}}$ | $W_{Lm}$ is the weight of limestone $W_{TOC}$ is the weight of total organic content | As above | Glorioso and Rattia (2012) |
| $B_{19} = \frac{W_{QFM} + W_{Cb}}{W_{Tot}} \approx \frac{W_{QFM} + W_{Cal} + W_{Dol}}{W_{Tot}}$ | $W_{QFM}$ is the weight of quartz, feldspar and mica $W_{Cb}$ is the weight of carbonate minerals including dolomite and calcite $W_{Cal}$ is the weight of calcite $W_{Tot}$ is the weight of total minerals | As above | Jin et al. (2014a, b) |

**Table 1** (continued)

| Formulae | Variable descriptions | Test methods | References |
|---|---|---|---|
| $B_{20} = \frac{w_{QFP}F_{QFP}}{w_{QFP}F_{QFP}+w_{Cb}F_{Cb}+w_{ClyTOC}F_{ClyTOC}+\phi w_{\phi}}$ | $w_{QFP}$, $w_{Cb}$, $w_{ClyTOC}$ and $w_{\Phi}$ are weighting factors<br>$F_{QFP}$, $F_{Cb}$ and $F_{ClyTOC}$ are the volume fractions; $\Phi$ is porosity | As above | Rybacki et al. (2016) |
| $B_{21} = -1.8748\phi + 0.9769$ | | Well log data or laboratory tests data | Jin et al., (2014a, b) |
| $B_{22} = \frac{H_{\mu}-H}{K}$ | $H_{\mu}$ and $H$ are the micro and macro indentation hardness<br>$K$ is the bulk modulus | Hardness test | Hucka and Das (1974) |
| $B_{23} = \frac{H_a}{K_c}$ | $H_a$ is the hardness<br>$K_c$ is the fracture toughness | Hardness test | Lawn and Marshall (1979) |
| $B_{24} = \frac{H_a \cdot E}{K_c^2}$ | | Hardness test | Quinn and Quinn (1997) |
| $B_{25} = \sin\theta = \frac{\mu}{\sqrt{1+\mu^2}}$ | $\theta$ is the internal friction angle<br>$\mu$ is the coefficient of internal friction | Mohr–Coulomb analysis | Hucka and Das (1974) |
| $B_{26} = \frac{F_{max}}{P}$ | $F_{max}$ is the maximum applied force<br>$P$ is the corresponding penetration | Penetration test | Yagiz (2009) |
| $B_{27} = \frac{P_{dec}}{P_{inc}}$ | $P_{dec}$ is the force decrement<br>$P_{inc}$ is the force increment | As above | Copur et al. (2003) |
| $B_{28} = q\sigma_c$ | $q$ is the percentage of fines ($-28$ mesh) | Impact test | Protodyakonov (1963) |
| $B_{29} = S_{20}$ | $S_{20}$ is the percentage of fines smaller than 11.2 mm | As above | Blindheim and Bruland (1998) |
| $B_{30} = K_b = \frac{\sigma_c}{P} - \frac{K_s}{h^2}$ | $K_b$ is the relative brittleness index<br>$P$ is the applied load at failure<br>$K_s$ is the shape factor<br>$h$ is the distance between loading points | Point load test | Reichmuth (1967) |
| $B_{31} = \frac{a - B_{31}\mathrm{Log}_{10}\mathrm{N(AEE)}}{\mathrm{Log}_{10}(\mathrm{AEE})}$ | AEE represents the energy of the AE event<br>N(AEE) is the accumulated number of AE events with energy not less than AEE<br>a is constant | Acoustic emission | Zhang et al. (2021) |
| $B_{32} = \frac{B_i - B_{min}}{B_{max} - B_{min}}$ | $B_i$ is the brittleness indexes before normalization, $B_i = B_{POST} + B_E$;<br>$B_E$ varies in the rage of 0–1, $B_{POST}$ is the post-peak brittleness index<br>$B_{max}$, $B_{min}$ are the maximum and minimum values for the brittleness indexes of rock specimens | Acoustic emission | Xia et al. (2017) |
| $B_{32} = \frac{\text{Compression conponent}}{\text{Tensile component}}$ | The compression component is estimated through UCS,<br>$UCS = \begin{cases} k\frac{A}{D^2}I_{s(nd)} \text{ for diametral} \\ k\frac{A}{4LD/}I_{s(na)} \text{ for axial} \end{cases}$<br>while the $I_{s(na)}$ and $I_{s(nd)}$ are substituted to tensile component | Point load test | Khadivi et al. (2023) |

does not take into account the effect of the rock strain path (Hajiabdolmajid and Kaiser 2003). Moreover, characterization of brittle behavior should be based not only on the effect of stress drop, but also on deformation characteristics.

Brittleness indices have therefore also been developed about the deformation behaviors of brittle rocks. Hucka and Das (1974) defined the brittleness index $B_6$ as a relationship between elastic strain and the total strain at failure. Based on the research of Andreev (1995), Rybacki et al. (2016) proposed a modified brittleness index, $B_7$, that utilizes the ratio of the difference between residual and peak strain to the residual strain. This index has a form similar to $B_5$; the former is based on strain and the latter on stress. Hajiabdolmajid and Kaiser (2003) suggested an approach for evaluating brittleness, index $B_8$, based on the correlation between the plastic strain when the friction strength is fully mobilized and the plastic strain when the cohesive strength reaches the value of the residual strength. However, the strain-dependent index $B_8$ does not account for the effect of strength evolution.

Brittleness in rocks can be measured by the ratio of elastic energy to total energy at failure—the brittleness index B9. Unfortunately, the index $B_9$ is defined only for the pre-peak stage; the energy development in the post-peak stage is ignored. Tarasov and Potvin (2013) developed an energy balance-based assessment approach that incorporates the behaviors in both the pre-peak and post-peak periods. The energy that corresponds to the complete stress–strain curve is classified into three types: the elastic energy stored within the specimen over the entire loading process, post-peak shear rupture energy and additional (or released) energy during failure. The rupture energy can be calculated as the amount of elastic energy plus the additional energy. Tarasov and Potvin (2013) defined the brittleness index $B_{10}$ as the ratio between the rupture energy and elastic energy, and $B_{11}$ as the ratio between the additional energy and elastic energy. These two indices can therefore be expressed as functions of the elastic modulus $E$ and the post-peak modulus $M$ for Class I and Class II behavior. However, the $B_{10}$ and $B_{11}$ indices present certain challenges; for instance, (1) different stress–strain curves may have the same $E$, $M$ and peak strength values but

different residual strength values, or (2) different stress–strain curves may have the same $E$, $M$ and strength drop values but different peak strength and residual strength values. Although these two indices can account for stress and strain performance, it is clear that these indices cannot be used to evaluate rock brittleness accurately.

To better evaluate rock brittleness, various methodologies accounting for strength, deformation, and pre- and post-peak behaviors have been proposed based on stress–strain curves. The brittleness index $B_{12}$ was proposed by Meng et al. (2015) based on the correlation between the magnitude of stress drop and the velocity of stress drop under conventional triaxial compression conditions. However, this index neglects the effect of pre-peak mechanical behavior when the peak and residual strength values and the difference between the two strain values are the same while the Young's modulus values are different.

## 2.2 Brittleness indices based on physical and mechanical characteristics

The Young's modulus ($E$) and Poisson's ratio ($\nu$) are the most widely used physical and mechanical characteristics for quantifying brittleness. According to Rickman et al. (2008), a relationship between the Poisson's ratio and Young's modulus can be determined to define the brittleness index $B_{13}$, which is based on the mean effects of the two parameters. What's more, these two static parameters can be derived from P waves, S waves and bulk density (Fjaer et al. 2008; Mullen et al. 2007). A higher Young's modulus and a lower Poisson's ratio of the rock may result in greater potential for brittle failure (Wang et al. 2015). Luan et al. (2014) proposed the brittleness index $B_{14}$, defined as the ratio of the Young's modulus to the Poisson's ratio. In addition, based on this ratio, the brittleness index $B_{15}$ was suggested by Sun et al. (2013) to consider rock density in the formula as well. Similar to $B_{14}$, a higher Young's modulus, lower Poisson's ratio and higher rock density would correspond to higher brittleness.

Mineralogical composition also plays a vital role in estimating rock brittleness. Brittleness indices based on mineral composition are calculated in terms of the ratios of the rock's contents. Several indices have been developed based on weight fractions.

For example, Jarvie et al. (2007) proposed the brittleness index $B_{16}$ as a function of brittle quartz and ductile carbonate and clay. The modified index $B_{17}$ was defined by Wang and Gale (2009) to incorporate the contributions of ductile limestone, brittle dolomite and total organic content. Glorioso and Rattia (2012) presented the index $B_{18}$, which accounts for the influence of total organic content and treats carbonates as brittle minerals. Jin et al. (2014a, b) described an improved brittleness index $B_{19}$ that includes the effects of silicate and carbonate minerals. The silicate minerals considered for this index include quartz, feldspar and mica, and the carbonate minerals include calcite and dolomite; all of these minerals were regarded as brittle. Composition-based indices can also be defined in terms of volume fractions. Rybacki et al. (2016) described a modified brittleness index $B_{20}$ that incorporates volume fractions, weighting factors and porosity. These workers also proposed a classification scheme for the strength of shales with three groups: mechanically strong = QFP, which includes quartz, feldspar and pyrite; intermediately strong = carbonate, and weak strength = Cly-TOC, which includes clay and total organic content.

Rock brittleness is also closely related to porosity, hardness and internal friction angle. Porosity has significant influence on deformation and strength behaviors, permeability evolution, and rock brittleness properties. Jin et al. (2014a, b) defined the brittleness index $B_{21}$ as a function of neutron porosity, which should be evaluated based on a large number of well log and/or laboratory data. Hardness properties, including macro- and micro-indentation hardness, were investigated to define the brittleness index $B_{22}$, as discussed by Hucka and Das (1974). The correlation between hardness and fracture toughness was examined by Lawn and Marshall (1979) to formulate the brittleness index $B_{23}$, which is determined by measuring resistance to deformation and fracturing to ceramic materials. Quinn and Quinn (1997) developed the brittleness index $B_{24}$ based on the ratio of deformation energy per unit volume and fracture surface energy per unit area. The internal friction angle-based brittleness index $B_{25}$ was proposed based on the Mohr–Coulomb failure criterion with regard to the pressure sensitivity of rock strength (Hucka and Das 1974). This index can be expressed two ways: in terms of the internal friction angle, or as a function of the coefficient of internal friction.

## 2.3 Brittleness indices based on special test parameters

Although many brittleness indices have been developed based on stress–strain curve tests and physical and mechanical characteristics, indices calculated from special test-based parameters have also been proposed that reflect the characteristics of fragility, cuttability, drillability, penetrability and fracability, which are important in rock engineering and mining sciences. Tests for determining these parameters include punch penetration tests, impact tests and point load tests. Yagiz (2009) proposed the rock brittleness classification scheme and the index $B_{26}$ based on the relationship between the maximum applied force and the corresponding penetration, which are widely applied in drilling and rock tunnel engineering. The brittleness index $B_{27}$ was quantified by Copur et al. (2003) using the ratio of the force decrement to the force increment. The $B_{28}$ index was defined by Protodyakonov (1963) using the impact test, based on the percentage of fines ($-28$ mesh) and the uniaxial compressive strength. The brittleness index $B_{29}$ was defined as the percentage of fines ($<11.2$ mm) formed in an impact test for TBM performance predicted with the NTNU model (Blindheim and Bruland 1998). Reichmuth (1967) proposed the brittleness index $B_{30}$ based on a point load test; the relative brittleness can be evaluated from the intercept and slope of the regression analysis of large amounts of experimental data. Zhang et al. (2021) propose a new exponent $B_{31}$ based on the rate of stress drop obtained from the post-peak stress–strain curve and the ratio of the elastic energy released during failure to the total energy stored before the peak strength, the energy being obtained by combining the relevant parameters of acoustic emission. Xia et al. (2017) proposed the AE parameter $B_{32}$ value to evaluate the state of fracture extension in rocks. This $B_{32}$ value is also a parameter that determines the fracture initiation point and the residual stress point.

As discussed above, many brittleness indices have been developed using a variety of approaches, and some have also been used extensively in rock excavation engineering and reservoir fracturing design. However, many of these indices have disadvantages. For example, some brittleness indices focus only on the stress or strain characteristics, some only reflect pre-peak or post-peak behaviors, and many neglect

the effects of confining pressure and pore pressure. Therefore, we aim to investigate the effects of confining pressure and pore pressure on the strength and brittleness of sandstone samples based on complete stress–strain curves under triaxial compression tests. This approach includes the integrated effect of stress and strain characteristics in both the pre-peak and post-peak periods.

## 3 Brittleness evaluation based on pre- and post-peak behaviors for stress–strain curves

### 3.1 The new brittleness index

The mechanical properties in the post-peak region play a vital role on the estimation of rock brittleness. A number of experimental investigations have been conducted into the post-peak behaviors of brittle rocks, and the results indicate that in general, rocks show significant stress drops and strain-softening behavior. Meng et al. (2015) evaluated rock brittleness based on post-peak characteristics, including the magnitude and velocity of the post-peak stress drop. Their results showed that the degree of brittleness decreased with increasing confining pressure. Although the brittleness index used accounted for post-peak behaviors, the effects of pre-peak behaviors were ignored. Therefore, selection of the appropriate parameters is of great importance to the evaluation of rock brittleness. A new brittleness index (BI) is herein proposed based on a stress–strain curve methodology that combines the stress and strain properties of both the pre- and post-peak regions.

This new brittleness index is determined based on the variations in stress and strain in the pre-peak and post-peak stages. The stress variation index $BI_1$ is defined as the ratio of the stress drop to the peak stress, which is equal to $B_5$. The stress drop is calculated as the peak stress minus the residual stress. The strain variation index $BI_2$ is the ratio of the difference between the variation in pre-peak strain and the variation in post-peak strain to the variation in pre-peak strain. The variation in pre-peak strain can be calculated as the peak strain minus the strain in the elastic stage that corresponds to a stress value equal to the residual stress. The variation in post-peak strain is measured as the residual strain minus the peak strain.

As shown in Fig. 1, the stress and strain parameters can be obtained from a simplified stress–strain curve.

BI can be expressed as follows:

$$\mathrm{BI} = \mathrm{BI}_1 \mathrm{BI}_2 = \frac{\sigma_\mathrm{p} - \sigma_\mathrm{r}}{\sigma_\mathrm{p}} \cdot \frac{2\varepsilon_\mathrm{p} - \varepsilon_\mathrm{r} - \varepsilon_\mathrm{m}}{\varepsilon_\mathrm{p} - \varepsilon_\mathrm{m}} \tag{1}$$

where $\varepsilon_\mathrm{m}$ is the strain in the elastic stage that corresponds to a stress value equal to the residual stress. $BI_1$ ranges from 0 to 1. When $BI_1$ is 0, the peak stress is equal to the residual stress, which implies that the rock exists in a ductile regime. When $BI_1$ is 1, the residual stress is 0, and the rock is in an absolute brittleness regime. Similarly, $BI_2$ ranges from $-\infty$ to 2. When $BI_2$ tends to $-\infty$, the peak strain tends to the strain in the elastic stage that corresponds to a stress value equal to the residual stress, the residual tends to $+\infty$, and it can be inferred that the rock is in a ductile regime. When $BI_2$ is 2, the residual strain is equal to the strain in the elastic stage that corresponds to the stress value equal to the residual stress, which indicates that the rock is in an absolute brittleness regime. In addition, when $BI_2$ is 1, the residual strain is equal to the peak strain, and the rock is in a brittleness regime. When $BI_2$ is 0, the variation in pre-peak strain is equal to the variation in post-peak strain, and the rock is in a semi-brittle regime. Because of the mechanical properties of the sandstone specimens, the variation in pre-peak strain is larger than the variation in post-peak strain in this study; the values of $BI_2$ range from 0 to 1. Consequently, the values of BI also range from 0 to 1, and a higher brittleness is implied for higher BI values.

### 3.2 Tested specimens and experiment apparatus

The rock blocks were quarried from a rock excavation in the southeast of Chongqing, Southwest China. The blocks were then transported to the State Key Laboratory of Coal Mine Disaster Dynamics and Control at Chongqing University, Chongqing, China. The sandstone core specimens were drilled and cut to a cylindrical shape 50 mm in diameter and 100 mm in length following the suggested methods of the International Society for Rock Mechanics. Photographs of representative prepared sandstone specimens are shown in Fig. 2.

The basic parameters of the collected specimens were assessed using two methods: proximate analysis and special surface area analysis. Proximate
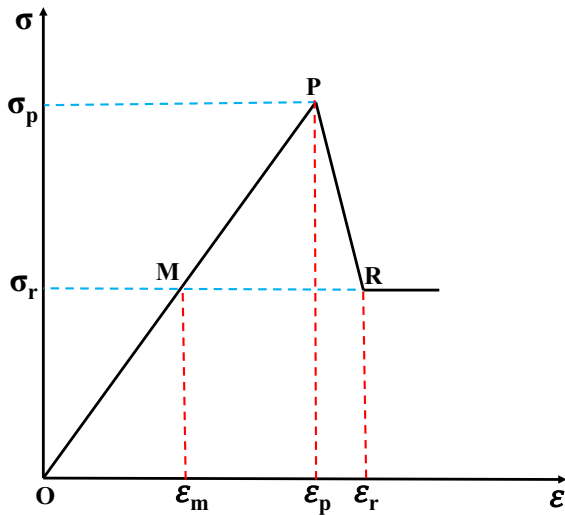
**Fig. 1** Schematic diagram of a simplified stress–strain curve

analysis is used to analyze the unknowns, unknown compositions and so on. The results are as follows: the sandstone used in the test is feldspathic coarse sandstone, with an apparent density of 2350 kg/m$^3$, and its mineral composition mainly consists of feldspar and quartz, with the content of quartz less than 75%, feldspar more than 25%, and the content of rock fragments less than 25%, which is grayish-white in color. Special surface area analysis refers to the testing of the pore structure of sandstone using a fully automated specific surface area analyzer. The results of these analyses are shown in Table 2; these data indicate a high ash content on an air-dried basis. Key physical properties of the sandstone samples were also evaluated for this study, such as their density and porosity. The values for two properties of the studied sandstone specimens, their sizes and corresponding triaxial compressive loading stress conditions, are listed in Table 3. The densities of tested sandstone specimens range from 2.34 to 2.52 g/cm$^3$; the values for porosity range from 9.62 to 10.78%.

In addition, the basic mechanical properties of the sandstone specimens were determined using uniaxial compression and Brazilian tensile tests. The results of these tests, listed in Table 4, indicate that the average uniaxial compressive strength (UCS) of the rock is 49.51 MPa, and that the average Brazilian tensile strength (BTS) is 6.38 MPa.

The triaxial compressive experiments were conducted with the thermal-hydrological- mechanical coupled with triaxial servo-controlled seepage apparatus for gas infiltrated coal and rock (shown in Fig. 3), developed by Yin et al. (2013) at Chongqing University, China. The servo loading system can provide a loading capacity of 1000 kN and a variety of control forms including the displacement control mode, force control mode and the program control mode. The triaxial pressure chamber has the capacity to withstand a maximum confining pressure of 60 MPa applied through a hydraulic pressure system. The gas pressure control system, which has a maximum gas pressure of 20 MPa, is used for the triaxial compression tests. The axial displacement and lateral deformation can be monitored by the linear variable differential transformer sensor and the circumferential extensometer, respectively, with a maximum axial displacement of 60 mm and radical deformation of 12 mm. All stress and deformation testing data can be acquired and recorded automatically by the data acquisition and storage system.

**Fig. 2** Photographs of prepared sandstone specimens

**Table 2** Characteristic parameters of the sandstone specimens

| Property | Value |
|---|---|
| Mad—moisture content on air dried basis (%) | 0.66 |
| Aad—ash content on air dried basis (%) | 95.9 |
| Vad—volatile content on air dried basis (%) | 3.19 |
| FCad—fixed carbon content on air dried basis (%) | 0.25 |
| BET surface area ($m^2/g$) | 3.0527 |
| Langmuir surface area ($m^2/g$) | 4.1646 |

The triaxial compression test is loaded in a stress-controlled manner at a rate of 0.01 MPa/s before the peak is reached, and in a displacement-controlled manner at a rate of 0.00167 mm/s after the peak is reached. Gas pressure was injected by the gas pressure control system after the specimen reached the specified triaxial condition, and the compression test was performed until the specimen had fully adsorbed the gas. A series of confining pressures of 10, 15, 20, 25 and 30 MPa and gas pressures of 0, 2, 3, 4 and 5 MPa were applied for triaxial compression tests. Stress–strain curves for sandstone under different confining pressures and gas pressures are shown in Fig. 4. Since $B_5$, $B_7$, $B_{10}$ and $B_{12}$ consider the effects of stress, strain, curve line shape and post-peak stress drop on brittleness, respectively, a comparative analysis with BI is carried out to evaluate the new brittleness index BI. The stress and strain parameters utilized in the newly developed brittleness index were calculated and are listed in Table 5. This table also includes the results for the brittleness indices $B_5$, $B_7$, $B_{10}$, $B_{12}$ and BI.

**Table 3** Characteristic parameters of the sandstone specimens

| Sample no | Diameter (mm) | Length (mm) | Density (g/cm³) | Porosity (%) | Confining pressure (MPa) | Gas pressure (MPa) |
|---|---|---|---|---|---|---|
| SS-1 | 49.78 | 96.2 | 2.34 | 3.93 | 10 | 0 |
| SS-2 | 50.0 | 95.9 | 2.37 | 4.16 | 10 | 2 |
| SS-3 | 49.8 | 97 | 2.42 | 4.24 | 10 | 3 |
| SS-4 | 49.4 | 95.9 | 2.39 | 4.28 | 10 | 4 |
| SS-5 | 49.8 | 91.68 | 2.36 | 3.83 | 10 | 5 |
| SS-6 | 49.78 | 96 | 2.40 | 4.25 | 15 | 0 |
| SS-7 | 49.6 | 100.5 | 2.35 | 4.19 | 15 | 2 |
| SS-8 | 49.5 | 99.3 | 2.43 | 4.22 | 15 | 3 |
| SS-9 | 49.5 | 97.9 | 2.35 | 3.96 | 15 | 4 |
| SS-10 | 49.5 | 100.9 | 2.45 | 4.16 | 15 | 5 |
| SS-11 | 49.89 | 98.6 | 2.38 | 3.85 | 20 | 0 |
| SS-12 | 49.78 | 97 | 2.44 | 4.29 | 20 | 2 |
| SS-13 | 48.6 | 100.2 | 2.51 | 4.15 | 20 | 3 |
| SS-14 | 49.5 | 98.7 | 2.36 | 4.24 | 20 | 4 |
| SS-15 | 49.5 | 100 | 2.47 | 3.88 | 20 | 5 |
| SS-16 | 49.78 | 94.64 | 2.52 | 4.34 | 25 | 0 |
| SS-17 | 49.8 | 95.4 | 2.43 | 4.25 | 25 | 2 |
| SS-18 | 48.8 | 100.8 | 2.39 | 4.17 | 25 | 3 |
| SS-19 | 49.5 | 100.4 | 2.41 | 4.22 | 25 | 4 |
| SS-20 | 48.6 | 99.52 | 2.38 | 3.86 | 25 | 5 |
| SS-21 | 49.78 | 97.4 | 2.34 | 4.13 | 30 | 0 |
| SS-22 | 49.58 | 101.3 | 2.38 | 3.92 | 30 | 2 |
| SS-23 | 49.7 | 100.4 | 2.37 | 4.03 | 30 | 3 |
| SS-24 | 49.6 | 101.4 | 2.35 | 3.95 | 30 | 4 |
| SS-25 | 48.44 | 100.7 | 2.40 | 3.98 | 30 | 5 |

**Table 4** Basic mechanical properties of the sandstone specimens

| Sample no | Diameter (mm) | Density (g/cm$^3$) | Porosityc (%) | UCS (MPa) | Young's modulus (GPa) | Poisson's ratio | BTS (MPa) |
|---|---|---|---|---|---|---|---|
| 1 | 49.5 | 2.38 | 10.63 | 56.31 | 4.30 | 0.26 | 6.42 |
| 2 | 49.8 | 2.36 | 9.88 | 48.9 | 4.13 | 0.27 | 6.37 |
| 3 | 49.8 | 2.41 | 10.46 | 43.32 | 4.05 | 0.25 | 6.34 |



**Fig. 3** Photograph of the experimental system

### 3.3 Verification and comparison of brittleness indices

The variation in the brittleness indices of the sandstone samples determined from the stress–strain curves for different confining pressures are presented in Fig. 5. The brittleness shows a strong sensitivity to stress, and BI decreases with increasing confining pressure, as shown in Fig. 5e. Various investigations have demonstrated that the confining pressure has significant influence on rock strength and brittleness, and that confining pressure is negatively correlated with rock brittleness. $B_5$, $B_{12}$, and the new brittleness index BI (Fig. 5a, d, e) show the same pattern: the

sandstone brittleness gradually decreases and plateaus as the surrounding pressure increases. Whereas $B_7$ (Fig. 5b) does not reflect such a pattern, $B_{10}$ (Fig. 5c) shows an approximate trend, except for samples tested at $\sigma_3 = 20$ MPa and $p = 3$ MPa. In $B_5$, the effect of gas pressure is reflected at low envelope pressures, while the effect of gas pressure is less at high envelope pressures; in $B_{12}$, the effect of gas pressure is reflected at different envelope pressures, but there is no difference in brittleness between the two at gas pressures of 0 and 1 MPa; in the new brittleness index BI, the change in brittleness characteristics of the sandstone is indicated at different gas pressures. Nevertheless, $B_5$ considers only the magnitude of stress drop and ignores the effect of strain in both the pre- and post-peak regimes. $B_{10}$ considers only the elastic modulus and the post-peak modulus and ignores the effects of peak stress and residual stress. $B_{12}$ consider the influence of the stress and strain behaviors in the post-peak stage and neglects the pre-peak strain. For our formula, both stress and strain behaviors in both the pre- and post-peak stages are account for, and the formula produces expected brittleness values.

The variation of the brittleness indices of the sandstone samples determined from the stress–strain curves for various gas pressures is shown in Fig. 6. In Fig. 6e, BI shows an increasing trend caused by increasing gas pressure. $B_5$ and $B_{12}$ show similar trends to BI (Fig. 6a, d). $B_{10}$ exhibits a trend that is approximately similar to these except for the samples tested at $\sigma_3 = 20$ MPa and $p = 3$ MPa (Fig. 6c). Similar to the correlation between $B_7$ and confining pressure, the relationship between $B_7$ and gas pressure is poor, and to some extent, $B_7$ demonstrates an unexpected trend (Fig. 6b). Previous experimental research has indicated a trend of strength reduction caused by $CO_2$ pressure (Perera et al. 2011). According to the effective stress law, the effective confining pressure can be calculated as the confining pressure minus the gas
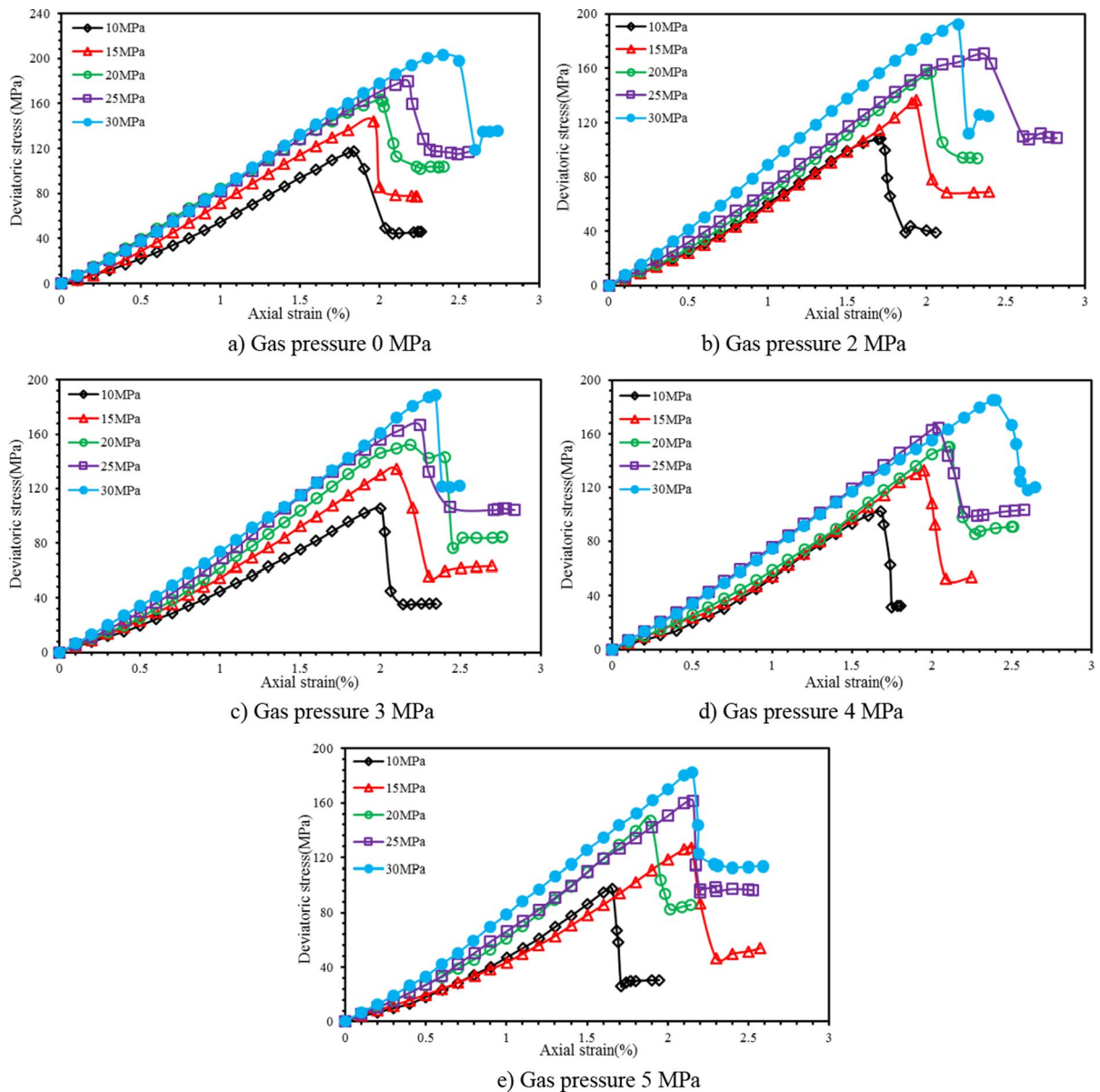
a) Gas pressure 0 MPa

b) Gas pressure 2 MPa

c) Gas pressure 3 MPa

d) Gas pressure 4 MPa

e) Gas pressure 5 MPa

**Fig. 4** Stress–strain curves of sandstone under different confining pressures and gas pressures

pressure, which would imply a decreasing effective confining pressure with increasing gas pressure. Consequently, relative to the confining pressure, the gas pressure has the opposite effect on strength, which was verified in this study by the results of the triaxial compression tests under different gas pressures. Furthermore, this finding indicates that higher gas pressure is associated with higher brittleness. Because of the limitations of $B_5$, $B_7$, $B_{10}$ and $B_{12}$, these four

brittleness indices cannot produce accurate estimations, whereas the proposed brittleness index is able to predict the correct values. Moreover, these results show that the influence of gas pressure on brittleness decreases with increasing confining pressure.

The results of the triaxial tests under confining pressure and gas pressure reveal significant pressure dependence of the stress drop and strain variation of stress–strain curves. These results imply that both

**Table 5** Summarized results for mechanical parameters and the brittleness indices $B_5$, $B_7$, $B_{10}$, $B_{12}$ and BI of sandstone under confining pressure and gas pressure

| Sample no | $\sigma_3$ (MPa) | $p$ (MPa) | $\sigma_p$ (MPa) | $\varepsilon_p$ (%) | $\sigma_r$ (MPa) | $\varepsilon_r$ (%) | $\varepsilon_m$ (%) | $B_5$ | $B_7$ | $B_{10}$ | $B_{12}$ | BI |
|---|---|---|---|---|---|---|---|---|---|---|---|---|
| SS-1 | 10 | 0 | 127.621 | 1.839 | 56.017 | 2.054 | 0.886 | 0.561 | 0.105 | 0.791 | 0.142 | 0.434 |
| SS-2 | 10 | 2 | 118.037 | 1.712 | 49.226 | 1.868 | 0.728 | 0.583 | 0.083 | 0.844 | 0.154 | 0.491 |
| SS-3 | 10 | 3 | 115.362 | 1.999 | 45.106 | 2.140 | 0.920 | 0.609 | 0.066 | 0.884 | 0.164 | 0.529 |
| SS-4 | 10 | 4 | 112.155 | 1.682 | 42.327 | 1.784 | 0.823 | 0.623 | 0.058 | 0.902 | 0.176 | 0.548 |
| SS-5 | 10 | 5 | 107.507 | 1.655 | 38.904 | 1.742 | 0.898 | 0.638 | 0.050 | 0.918 | 0.185 | 0.565 |
| SS-6 | 15 | 0 | 158.917 | 1.965 | 92.688 | 2.200 | 1.080 | 0.417 | 0.107 | 0.713 | 0.102 | 0.306 |
| SS-7 | 15 | 2 | 151.346 | 1.936 | 83.577 | 2.130 | 1.130 | 0.448 | 0.091 | 0.775 | 0.114 | 0.340 |
| SS-8 | 15 | 3 | 149.690 | 2.095 | 73.195 | 2.285 | 1.067 | 0.511 | 0.083 | 0.822 | 0.133 | 0.416 |
| SS-9 | 15 | 4 | 147.591 | 1.949 | 67.762 | 2.091 | 1.110 | 0.541 | 0.068 | 0.866 | 0.149 | 0.450 |
| SS-10 | 15 | 5 | 142.036 | 2.147 | 61.965 | 2.314 | 1.068 | 0.564 | 0.072 | 0.862 | 0.151 | 0.476 |
| SS-11 | 20 | 0 | 183.745 | 2.011 | 123.966 | 2.251 | 1.223 | 0.325 | 0.107 | 0.634 | 0.078 | 0.226 |
| SS-12 | 20 | 2 | 177.121 | 2.027 | 113.998 | 2.230 | 1.308 | 0.356 | 0.091 | 0.719 | 0.089 | 0.256 |
| SS-13 | 20 | 3 | 172.370 | 2.247 | 103.786 | 2.510 | 1.236 | 0.398 | 0.105 | 0.706 | 0.096 | 0.294 |
| SS-14 | 20 | 4 | 170.370 | 2.110 | 101.825 | 2.273 | 1.305 | 0.402 | 0.071 | 0.809 | 0.106 | 0.321 |
| SS-15 | 20 | 5 | 167.133 | 1.891 | 99.349 | 2.009 | 1.259 | 0.406 | 0.059 | 0.846 | 0.112 | 0.330 |
| SS-16 | 25 | 0 | 204.791 | 2.181 | 141.305 | 2.449 | 1.372 | 0.310 | 0.109 | 0.604 | 0.074 | 0.207 |
| SS-17 | 25 | 2 | 195.600 | 2.335 | 134.579 | 2.611 | 1.425 | 0.312 | 0.106 | 0.621 | 0.073 | 0.217 |
| SS-18 | 25 | 3 | 191.685 | 2.247 | 131.353 | 2.435 | 1.465 | 0.315 | 0.077 | 0.735 | 0.079 | 0.239 |
| SS-19 | 25 | 4 | 189.070 | 2.043 | 126.428 | 2.203 | 1.303 | 0.331 | 0.073 | 0.763 | 0.086 | 0.260 |
| SS-20 | 25 | 5 | 186.450 | 2.155 | 123.530 | 2.294 | 1.458 | 0.337 | 0.060 | 0.810 | 0.090 | 0.271 |
| SS-21 | 30 | 0 | 233.324 | 2.400 | 164.707 | 2.703 | 1.527 | 0.294 | 0.112 | 0.571 | 0.069 | 0.192 |
| SS-22 | 30 | 2 | 222.785 | 2.237 | 155.890 | 2.512 | 1.372 | 0.300 | 0.109 | 0.591 | 0.072 | 0.205 |
| SS-23 | 30 | 3 | 218.845 | 2.342 | 151.598 | 2.585 | 1.401 | 0.307 | 0.094 | 0.662 | 0.075 | 0.228 |
| SS-24 | 30 | 4 | 215.228 | 2.383 | 147.938 | 2.602 | 1.521 | 0.313 | 0.084 | 0.706 | 0.078 | 0.233 |
| SS-25 | 30 | 5 | 212.611 | 2.152 | 145.152 | 2.284 | 1.574 | 0.317 | 0.058 | 0.806 | 0.086 | 0.245 |

confining pressure and gas pressure play important roles in determining rock brittleness and the stress and strain behaviors in the pre-peak and post-peak stages. Many more factors also influence rock brittleness, such as temperature, loading rate and effective differential stress. Ideally, laboratory conditions should evaluate and control more boundary conditions, such as stress, temperature and loading rate. Of course, laboratory conditions represent simplifications of in-situ conditions, and the differences between these conditions must be considered. It is also important to note that the stress–strain curve-based brittleness indices depend strongly on the stiffness of experimental machinery and the appropriate selection of the pre- and post-peak parameters. Furthermore, brittle behavior would respond differently in different types of rock. Therefore, further study of brittleness index evaluation for different types of

rock is still necessary. Rock is often under true triaxial stress conditions in practical engineering, so the established brittleness index should conform to the true triaxial stress situation. The effects of stress loading rate, intermediate principal stresses and temperature on the brittleness index at this point need to be investigated in more detail.

## 4 Conclusions

Brittleness is an important property of rock that has extensive applicability in rock excavation engineering and reservoir fracturing. A variety of indices for the evaluation of brittleness were summarized and grouped into three categories based on the different rock mechanics considered for their formulae. In general, the definition of rock brittleness should
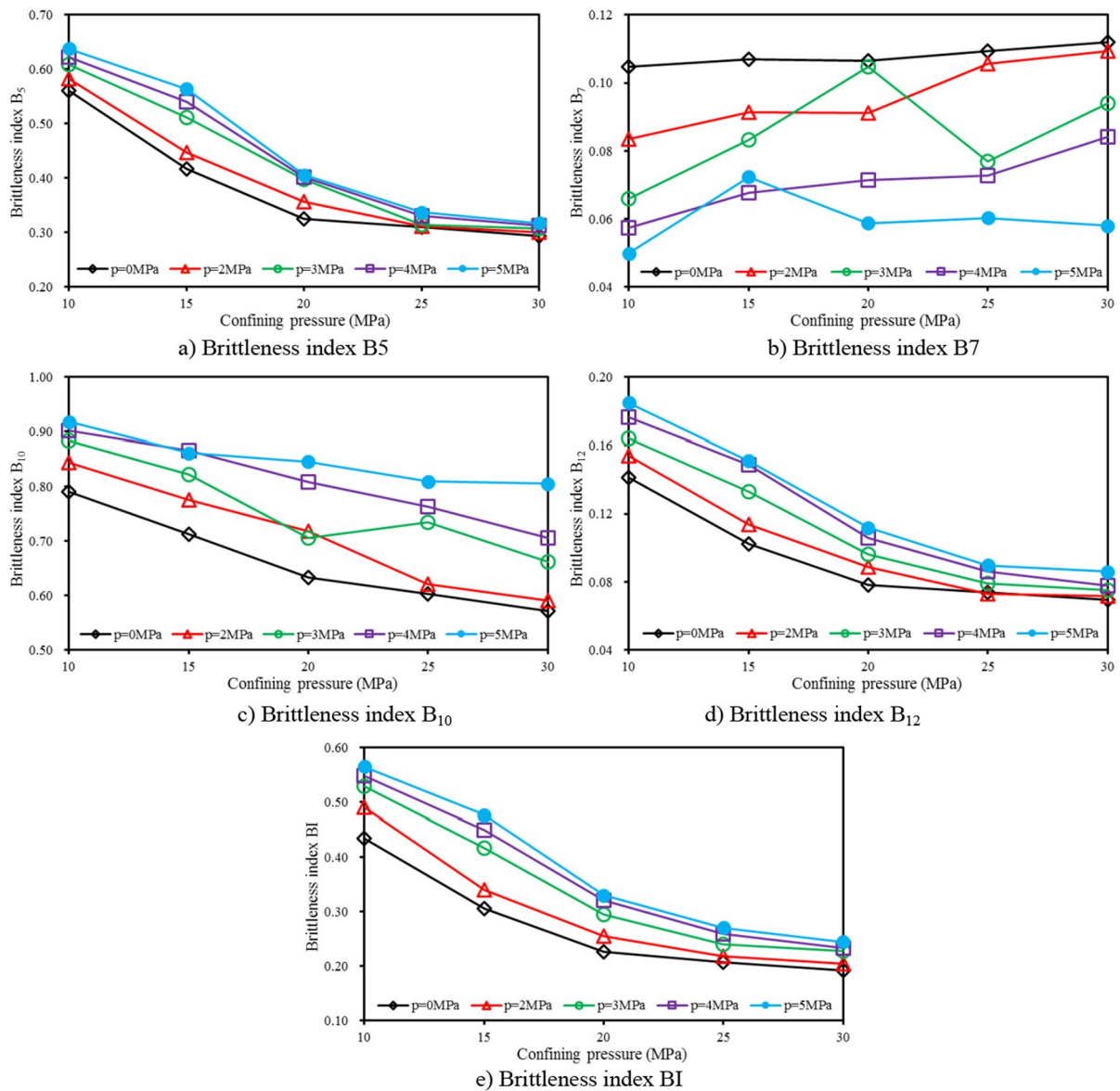
a) Brittleness index B5

b) Brittleness index B7

c) Brittleness index $B_{10}$

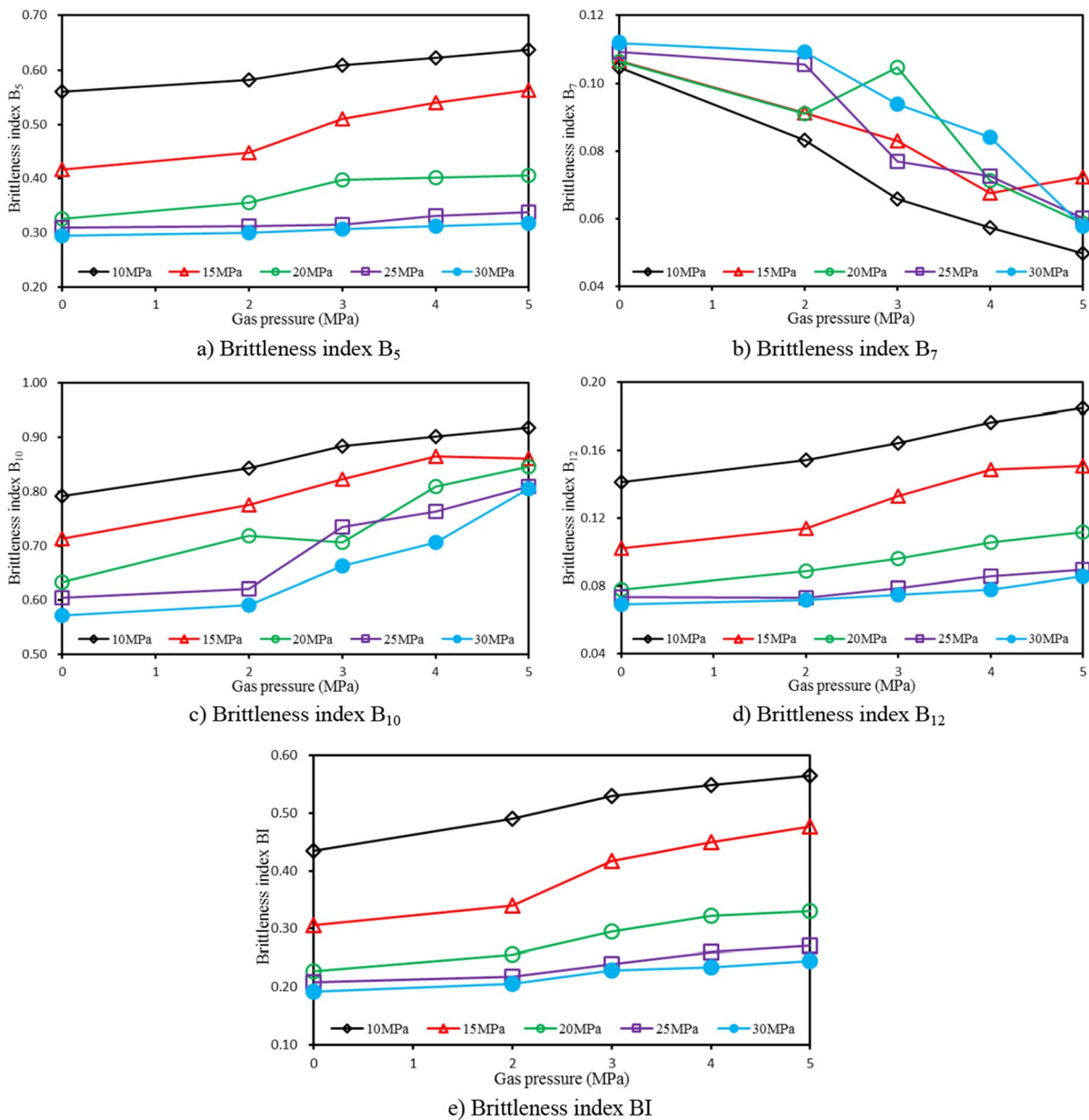d) Brittleness index $B_{12}$

e) Brittleness index BI

**Fig. 5** The relationships between the brittleness indices $B_5$, $B_7$, $B_{10}$, $B_{12}$ and BI and the confining pressure of sandstone under different gas pressures

be based on rock failure; however, no consensus has yet been reached on the precise definition or method of measuring rock brittleness. Therefore, we have proposed a new method for estimating rock brittleness that is based on stress–strain curves and on the rock behaviors that occur both before and after rock failure.

We note that the existing stress–strain curve-based brittleness indices would be able to evaluate brittleness more effectively if the parameters used represented unique and certain stress–strain curves. The newly proposed index is therefore based on the stress drop and a strain ratio that represents the relationship between the elastic strain and post-peak

**Fig. 6** The relationships between the brittleness indices $B_5$, $B_7$, $B_{10}$, $B_{12}$ and BI and the gas pressure of sandstone under different confining pressures

strain, which together combine the variation in stress with the variation in strain for both the pre- and post-peak stages. Triaxial compression tests of sandstone under different confining pressures and gas pressures were conducted, and key stress and strain parameters were recorded. Based on comparison of a variety of brittleness indices, as well as

further analysis, our results indicate that the newly proposed brittleness index can more effectively estimate rock brittleness.

The relationship between rock brittleness and confining pressure was also investigated, and our findings indicate that confining pressure is negatively associated with brittleness in sandstone. The correlation

between the rock brittleness and gas pressure implies that gas pressure is positively associated with brittleness in sandstone. Therefore, lower confining pressure and a higher gas pressure would result in higher brittleness for sandstone. The above research will provide a better description of the mechanical behaviour of the rock and clarify the force characteristics of the rock and ensure the safety of the project. However, there are still many factors that have not been considered in conventional triaxial testing of sandstones and the effect of these factors on rock brittleness needs to be further investigated.

**Author contributions**  WL and JW wrote the main manuscript text; JD was mainly involved in the content improvement and revision of the article; XC, TW, HZ and RH prepared Figs. 1–6 and Tables 1–6. All authors reviewed the manuscript.

**Availability of data and materials**  The data that support the findings of this study are available from the corresponding author (Wenpu Li) upon reasonable request.

**Declarations**

**Ethics approval and consent to participate**  There are no ethical issues related to the research in this paper.

**Consent for publication**  Not applicable.

**Competing interests**  The authors declare no competing interests.

# References

Altindag R (2002) The evaluation of rock brittleness concept on rotary blast hole drills. J S Afr Inst Min Metall 102:61–66

Andreev GE (1995) Brittle failure of rock materials: test results and constitutive models George E. A. A. Balkema, Rotterdam, p 446

Bai X, Zhang D, Zeng S, Zhang S, Wang D, Wang FL (2020) An enhanced coalbed methane recovery technique based on $CO_2$ phase transition jet coal-breaking behavior. Fuel 265:116912

Bishop AW (1967) Progressive failure with special reference to the mechanism causing it. Proc Geotech Conf Oslo 2:142–150

Blindheim OT, Bruland A (1998) Boreability testing, Norwegian TBM tunneling 30 years of experience with TBMs in Norwegian tunneling. Norwegian soil and rock engineering association publication no. 11, Trondheim, pp 29–34

Chen FJ, Li HX, Zhu ZQ (2012) Energy dissipation analysis on unloading confining pressure failure process of rock material. AMM 398:256–259

Chen PQ, Cui JT, Zhou XJ (2013) Research on effects of pressure loading on rock lateral cracks occurrence under confining pressure. AMR 850:838–841

Copur H, Bilgin N, Tuncdemir H, Balci C (2003) A set of indices based on indentation tests for assessment of rock cutting performance and rock properties. J S Afr Inst Min Metall 103(9):589–599

Du F, Wang K, Wang G, Jiang Y, Xin C, Zhang X (2018) Investigation of the acoustic emission characteristics during deformation and failure of gas-bearing coal-rock combined bodies. J Loss Prev Process Ind 55:253–266

Duan M, Jiang C, Yin WZ, Yang K, Li J, Liu Q (2021) Experimental study on mechanical and damage characteristics of coal under true triaxial cyclic disturbance. Eng Geol 295:106445

Dursun AE, Gokay MK (2016) Cuttability assessment of selected rocks through different brittleness values. Rock Mech Rock Eng Rock Mech Rock Eng 49:1173–1190

Fjaer E, Holt RM, Hordrud P, Raaen AM, Risnes R (2008) Petroleum related rock mechanics. Elsevier Press, London

Glorioso JC, Rattia A (2012) Unconventional reservoirs: basic petrophysical concepts for shale gas. SPE Pap 153004:36

Hajiabdolmajid V, Kaiser P (2003) Brittleness of rock and stability assessment in hard rock tunneling. Tunn Undergr Space Technol 18(1):35–48

Holt RM, Fjaer E, Stenebraten JF, Nes OM (2015) Brittleness of shales: relevance to borehole collapse and hydraulic fracturing. J Pet Sci Eng 131:200–209

Holt RM, Fjaer E, Nes OM, Alassi HT (2011) In: 45th US rock mechanics/geomechanics symposium, 2011. A Shaly Look at Brittleness. American Rock Mechanics Association

Hucka V, Das B (1974) Brittleness determination of rocks by different methods. Int J Rock Mech Min Sci Geomech Abstr 11(10):389–392

Jarvie DM, Hill RJ, Ruble TE, Pollastro RM (2007) Unconventional shale-gas systems: the Mississippian Barnett Shale of north-central Texas as one model for thermogenic shale-gas assessment. AAPG Bull 91(4):475–499

Jin X, Shah SN, Roegiers JC, Zhang B (2014a) Fracability evaluation in shale reservoirs an integrated petrophysics and geomechanics approach. In: Proceedings of the SPE hydraulic fracturing technology conference. Society of Petroleum Engineers

Jin X, Shah SN, Truax JA, Roegiers JC (2014b) A practical petrophysical approach for brittleness prediction from porosity and sonic logging in shale reservoirs. In: SPE annual technical conference and exhibition. Society of Petroleum Engineers

Khadivi B, Masoumi H, Heidarpour A, Zhang Q, Zhao J (2023) Assessing the fracturing process of rocks based on burst-brittleness ratio (BBR) governed by point load testing. Rock Mech Rock Eng 56:8167–8189

Kong XG, Wang EY, Hu SB, Li ZH, Liu XF, Fang BF, Zhan TQ (2015) Critical slowing down on acoustic emission characteristics of coal containing methane. J Nat Gas Sci Eng 24:156–165

Lawn BR, Marshall DB (1979) Hardness, toughness, and brittleness: an indentation analysis. J Am Ceram Soc 62:347–350

Li X, Li Q, Hu Y, Teng L, Yang S (2021) Evolution characteristics of mining fissures in overlying strata of stope after converting from open-pit to underground. Arab J Geosci 14:1–8

Li XS, Peng J, Xie YL, Li QH, Zhou T, WangJ W, Zheng WB (2022b) Influence of high-temperature treatment on strength and failure behaviors of a quartz-rich sandstone under true triaxial condition. Lithosphere 2022(Special 10):3086647

Li X, Peng J, Xie Y, Li Q, Zhou T, Wang J, Zheng W (2022) Influence of high-temperature treatment on strength and failure behaviors of a quartz-rich sandstone under true triaxial condition. Lithosphere

Liu ZB (2013) Experimental research of fine sandstone strength and deformation characteristics under different confining and hydraulic pressure. AMM 562:353–356

Liu JS, Wang JG, Chen ZW, Wang SG, Elsworth D, Jiang YD (2011) Impact of transition from local swelling to macro swelling on the evolution of coal permeability. Int J Coal Geol 88:31–40

Luan X, Di B, Wei J, Li X, Qian K, Xie J, Ding P (2014) Laboratory measurements of brittleness anisotropy in synthetic shale with different cementation. In: Proceedings of the 2014 SEG annual meeting. Denver, Society of Exploration Geophysicists. pp 3005–3009

Meng FZ, Zhou H, Zhang C, Xu R, Lu J (2015) Evaluation methodology of brittleness of rock based on post-peak stress–strain curves. Rock Mech Rock Eng 48(5):1787–1805

Mullen MJ, Roundtree R, Turk GA (2007) A composite determination of mechanical rock properties for stimulation design (what to do when you don't have a sonic log). Society of Petroleum Engineers, Denver

Pan Z, Connell LD (2007) A theoretical model for gas adsorption-induced coal swelling. Int J Coal Geol 69:243–252

Perera MSA, Ranjith PG, Peter M (2011) Effects of saturation medium and pressure on strength parameters of Latrobe valley brown coal: carbon dioxide, water and nitrogen saturations. Energy 36:6941–6947

Protodyakonov MM (1963) Mechanical properties and drillability of rocks. In: Proceedings of the 5th symposium rock mechanics. University of Minnesota, pp 103–118

Quinn JB, Quinn GD (1997) Indentation brittleness of ceramics: a fresh approach. J Mater Sci 32:4331–4346

Ranjith PG, Jasinge D, Choi SK, Mehic M, Shannon B (2010) The effect of $CO_2$ saturation on mechanical properties of Australian black coal using acoustic emission. Fuel 89(8):2110–2117

Reichmuth DR (1967) Point load testing of brittle materials to determine tensile strength and relative brittleness. In: The 9th US symposium on rock mechanics (USRMS). American Rock Mechanics Association, pp 134–159

Rickman R, Mullen M, Grieser B, Kundert D (2008) A practical use of shale petrophysics for stimulation design optimization: all shale plays are not clones of the Barnett shale. SPE Pap 115258:11

Rybacki E, Reinicke A, Meier T, Makasi M, Dresen G (2015) What controls the mechanical properties of shale rocks?—Part I: strength and Young's modulus. J Pet Sci Eng 135:702–722

Rybacki E, Meier T, Dresen G (2016) What controls the mechanical properties of shale rocks?—Part II: brittleness. J Pet Sci Eng 144:39–58

Sun SZ, Wang KN, Yang P, Li XG, Sun JX, Liu BH, Jin K (2013) Integrated prediction of shale oil reservoir using pre-stack algorithms for brittleness and fracture detection. In: Beijing, international petroleum technology conference

Tarasov B, Potvin Y (2013) Universal criteria for rock brittleness estimation under triaxial compression. Int J Rock Mech Min Sci 59:57–69

Vishal V, Ranjith PG, Singh TN (2015) An experimental investigation on behaviour of coal under fluid saturation, using acoustic emission. J Nat Gas Sci Eng 22:428–436

Wang FP, Gale JF (2009) Screening criteria for shale-gas systems. Trans Gulf Coast Assoc Geol Soc 59:779–793

Wang D, Ge H, Wang X, Wang J, Meng F, Suo Y, Han P (2015) A novel experimental approach for fracability evaluation in tight-gas reservoirs. J Nat Gas Sci Eng 23:239–249

Wang G, Liu Z, Wang P, Guo Y, Wang W, Huang T, Li W (2019) The effect of gas migration on the deformation and permeability of coal under the condition of true triaxial stress. Arab J Geosci 12:1–12

Wang W, Cao G, Li Y, Zhou Y, Lu T, Wang Y, Zheng B (2022) Experimental study of dynamic characteristics of tailings with different reconsolidation degrees after liquefaction. Front Earth Sci 10:876401

Wu Z, Zhang P, Fan L, Liu Q (2019) Numerical study of the effect of confining pressure on the rock breakage efficiency and fragment size distribution of a TBM cutter using a coupled FEM-DEM method. Tunn Undergr Space Technol 88:260–275

Xia Y, Li L, Tang C, Li X, Ma S, Li M (2017) A new method to evaluate rock mass brittleness based on stress–strain curves of class I. Rock Mech Rock Eng 50:1123–1139

Xie J, Gao MZ, Yu B, Zhang R, Jin WC (2015) Coal permeability model on the effect of gas extraction within effective influence zone. Geomech Geophys Geo-Energy Geo-Resour 1:15–27

Xu D, Liu J, Wu Z, Wang L, Liu H, Xiao F, Zeng Y, Lyu C (2020) Experimental investigation on permeability evolution of dolomite caprock under triaxial compression. Energies 13:6535

Xue Y, Liu J, Ranjith PG, Gao F, Xie H, Wang J (2022) Changes in microstructure and mechanical properties of low-permeability coal induced by pulsating nitrogen fatigue fracturing tests. Rock Mech Rock Eng 55:1–20

Xue Y, Ranjith PG, Chen Y, Cai C, Gao F, Liu X (2023) Nonlinear mechanical characteristics and damage constitutive model of coal under $CO_2$ adsorption during geological sequestration. Fuel 331:125690

Yagiz S (2009) Assessment of brittleness using rock strength and density with punch penetration test. Tunn Undergr Space Technol 24(1):66–74

Yang Y, Sone H, Hows A, Zoback MD (2013) Comparison of brittleness indices in organic-rich shale formations. ARMA Pap 13–403:7

Yin GZ, Jiang CB, Wang JG, Xu J (2013) Combined effect of stress, pore pressure and temperature on methane permeability in anthracite coal: an experimental study. Transp Porous Media 100:1–16

Yin GZ, Jiang CB, Wang JG, Xu J (2015a) Geomechanical and flow properties of coal from loading axial stress and unloading confining pressure tests. Int J Rock Mech Min Sci 76:155–161

Yin GZ, Li MH, Wang JG, Xu J, Li WP (2015b) Mechanical behavior and permeability evolution of gas infiltrated coals during protective layer mining. Int J Rock Mech Min Sci 80:292–301

Zhang DC, Ranjith PG, Perera MSA (2016) The brittleness indices used in rock mechanics and their application in shale hydraulic fracturing: a review. J Pet Sci Eng 143:158–170

Zhang Z, Zhang R, Cao Z, Gao M, Zhang Y, Xie J (2020) Mechanical behavior and permeability evolution of coal under different mining-induced stress conditions and gas pressures. Energies 13:2677

Zhang H, Wang Z, Song Z, Zhang Y, Wang T, Zhao W (2021) Acoustic emission characteristics of different brittle rocks and its application in brittleness evaluation. Geomech Geophys Geo-Energy Geo-Resour 7:48